Published in final edited form as:
Mol Pharm. 2013 October 7; 10(10): 3871–3881. doi:10.1021/mp400342f.

Resveratrol-Loaded Nanoparticles Based on Poly(epsilon-caprolactone) and Poly(D,L-lactic-*co*-glycolic acid)–Poly(ethylene glycol) Blend for Prostate Cancer Treatment

Vanna Sanna[†,‡,§], **Imtiaz Ahmad Siddiqui**[‡,§], **Mario Sechi**[*,†,‡], and **Hasan Mukhtar**[*,‡]

[†]Department of Chemistry and Pharmacy, Laboratory of Nanomedicine, University of Sassari, 07100 Sassari, Italy

[‡]Department of Dermatology, Medical Sciences Center, University of Wisconsin—Madison, 1300 University Avenue, Madison, Wisconsin 53706, United States

Abstract

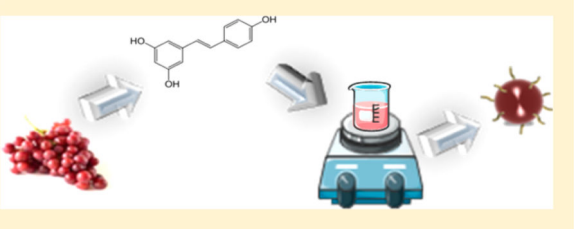

Nanoencapsulation of antiproliferative and chemopreventive phytoalexin *trans*-resveratrol (RSV) is likely to provide protection against degradation, enhancement of bioavailability, improvement in intracellular penetration and control delivery. In this study, polymeric nanoparticles (NPs) encapsulating RSV (nano-RSV) as novel prototypes for prostate cancer (PCa) treatment were designed, characterized and evaluated using human PCa cells. Nanosystems, composed of a biocompatible blend of poly(epsilon-caprolactone) (PCL) and poly(D,L-lactic-*co*-glycolic acid)-poly(ethylene glycol) conjugate (PLGA-PEG-COOH), were prepared by a nanoprecipitation method, and characterized in terms of morphology, particle size and zeta potential, encapsulation efficiency, thermal analyses, and in vitro release studies. Cellular uptake of NPs was then evaluated in PCa cell lines DU-145, PC-3, and LNCaP using confocal fluorescence microscopy, and antiproliferative efficacy was assessed using MTT assay. With encapsulation efficiencies ranging from 74% to 98%, RSV was successfully loaded in PCL:PLGA-PEG-COOH NPs, which showed an average diameter of 150 nm. NPs were able to control the RSV release at pH 6.5 and 7.4, mimicking the acidic tumoral microenvironment and physiological conditions, respectively,

[*]**Corresponding Authors**, M. Sechi: Department of Chemistry and Pharmacy, Laboratory of Nanomedicine, University of Sassari, Via Vienna 2, 07100, Sassari, Italy. Tel: +39 079-228-753. Fax: +39 079 229-559. Laboratory of Nanomedicine, c/o Porto Conte Ricerche, Localita Tramariglio, Alghero 07041, Sassari, Italy. mario.sechi@uniss.it.. [*]H. Mukhtar: Department of Dermatology, University of Wisconsin, Medical Sciences Center, 1300 University Avenue, Madison, WI 53706, United States. Phone: 608 263 3927. Fax: 608 263 5223. hmukhtar@wisc.edu..
[§]VS. and I.A.S. contributed equally to this work.

Author Contributions
The authors declare no competing financial interest.

with only 55% of RSV released within 7 h. In gastrointestinal simulated fluids, NPs released about 55% of RSV in the first 2 h in acidic medium, and their total RSV content within the subsequent 5 h at pH 7.4. Confocal fluorescence microscopy observations revealed that NPs were efficiently taken up by PCa cell lines. Furthermore, nano-RSV significantly improved the cytotoxicity compared to that of free RSV toward all three cell lines, at all tested concentrations (from 10 μM to 40 μM), proving a consistent sensitivity toward both the androgen-independent DU-145 and hormone-sensitive LNCaP cells. Our findings support the potential use of developed nanoprototypes for the controlled delivery of bioactive RSV for Pca chemoprevention/chemotherapy.

Keywords

resveratrol; nanoparticles; poly(epsilon-caprolactone); poly(D,L-lactic-co-glycolic acid)-poly(ethylene glycol) conjugate; prostate cancer

INTRODUCTION

trans-Resveratrol (RSV), the natural phytoalexin present in grapes, berries, peanuts and red wine, is well-known for its antioxidant,[1] antiaging,[2,3] antiviral,[4] cardiovascular[5] and neuro-protective effects.[6] As far as the antiproliferative properties are concerned, in 1996, Jang and coauthors published the first article on the ability of RSV to inhibit initiation and promotion of induced skin cancer and progression of breast cancer in mice.[7] Since then, numerous studies demonstrated antiproliferative, anticancer and chemopreventive efficacy of RSV against of a wide variety of tumors including lymphoid,[8] myeloid,[9] breast,[10] prostate,[11,12] colon,[13] pancreas,[14] lung,[15] melanoma,[16] ovarian,[17] and cervical cancers.[18] In addition, it was also demonstrated that RSV directly modulates various molecular signal transduction pathways that are known to induce cancer cell death or to inhibit cancer cell proliferation.[19,20]

Many in vitro studies established that RSV inhibits the growth of LNCaP (hormone-sensitive cells), DU-145 (androgen-independent cells), and PC-3 (hormone-independent line possessing dysfunctional androgen receptors) prostate cancer (PCa) cell lines in a concentration-dependent manner.[21] RSV induces apoptosis in LNCaP and DU145 cells through different protein kinase (PK) C-mediated and mitogen-activated protein kinases (MAPK)-dependent pathways.[22] It has also been shown to reduce oxidative stress within premalignant cells, and to decrease the production of nitric oxide in PC-3 and DU-145 cells, thus reducing growth and spread of PCa.[23] The chemopreventive effect of RSV on PCa was also supported by animal studies.[24,25]

Regardless of the promising results, the extensive use of RSV has met only limited success, largely due to its instability, poor solubility, inefficient systemic delivery, and low bioavailability.[26,27] To overcome these physicochemical and pharmacokinetic limitations, the encapsulation of RSV into nanodevices is a major challenge, and nanotechnology represents a powerful strategy.[28–31] In fact, the nanoencapsulation of chemo-therapeutic agents, such as bioactive natural products, provide many advantages in the protection of degradation and interaction with the biological environment, as well as enhancement of

absorption, bioavailability, retention time, improvement of intracellular penetration and control delivery.[32–37]

Concerning the biopolymers to be used for the preparation of NPs, several studies demonstrated the effectiveness of poly(D,L-lactic-*co*-glycolic acid) (PLGA) as a promising biomaterial for many therapeutic application, with the potential to protect the loaded compounds from degradation, as well as to provide a sustained drug release.[38,39] Mechanistically, PLGA NPs are usually taken up by endocytosis, which then release the drug at intracellular locations resulting in enhanced therapeutic action and reduced side effects.[40,41]

Moreover, the rapid reticuloendothelial system (RES) uptake of PLGA NPs could be significantly reduced by modifying their surface with poly(ethylene glycol) (PEG) that prevents opsonin binding, prolongs the circulation time of nanosystems in the blood and allows their targeting to tissues.[42,43] Again, such constructs of size <200 nm with hydrophilic surfaces tend to exhibit an improved enhanced permeability and retention (EPR) effect, which has been attributed to the increased residence time of the carrier in blood.[44,45]

However, so far, only few RSV nanosystems for cancer treatment have been reported. In particular, RSV incorporated into mPEG-poly(epsilon-caprolactone)-based NPs showed higher cytotoxicity compared to free RSV against glioma cells.[46] On the other hand, RSV-bovine serum albumin NPs significantly inhibited the growth rate of subcutaneously implanted human primary ovarian carcinoma cells in nude mice.[47]

To continue our research program focused on the use of natural compounds on cancer chemoprevention of PCa,[48–50] in this study we propose a first example of biocompatible polymeric NPs encapsulating RSV as a potential carrier for PCa treatment.

To explore and to modulate the properties of the polymeric matrix, we envisioned to obtain nanosystems by a blend of two biocompatible polymers, poly(epsilon-caprolactone) (PCL) and poly(D,L-lactic-*co*-glycolic acid)-poly(ethylene glycol) (PLGA-PEG-COOH) conjugate. Subsequently, the target NPs were prepared, fully characterized and investigated by physicochemical techniques, encapsulation efficiency and in vitro release studies. Finally, cellular uptake of the fluorescent NPs was detected, and nano-RSV prototypes were evaluated for their ability to inhibit the growth of DU-145, PC-3, and LNCaP cells.

EXPERIMENTAL SECTION

Materials

For preparation of NPs, PLGA (lactide/glycolide ratio of 50:50, carboxylic acid end group, viscosity range: 0.20 dL/g) was kindly provided from Purac Biomaterials (Gorinchem, Netherlands). PCL, RSV powder and fluorescein-5-isothiocyanate (FITC) were purchased from Sigma-Aldrich (Steinheim,Germany). The heterofunctional PEG polymer with a terminal amine and carboxylic acid functional group, NH_2-PEG-COOH (MW = 3400), was purchased from JenKem Technology USA. All solvents and other chemicals were obtained from Sigma-Aldrich, were analytical grade and were used without further purification. Nuclear magnetic resonance (^{1}H NMR) spectra were determined in $CDCl_3$ and were

recorded at 500 MHz on a Bruker Avance 500. Chemical shifts are reported in parts per million (ppm) downfield from tetramethylsilane (TMS), used as an internal standard. The purity of copolymer was determined by high performance liquid chromatography (HPLC) using an HP 1200 (Agilent Technologies, U.S.) system equipped with a Hypersil BDS C18 column (Alltech Italy, 250 mm × 4.6 mm i.d., 5 μm particle size); this material was found to be >95% pure.

PLGA-PEG-COOH Conjugation

To a solution of PLGA-COOH (3.0 g, 0.166 mmol) in anhydrous methylene chloride (10 mL), were added *N*-hydroxysuccinimide (NHS, 76 mg, 0.66 mmol) and 1-ethyl-3-(3-dimethylaminopropyl)-carbodiimide (EDC, 140 mg, 0.72 mmol), and the reaction mixture was magnetically stirred at room temperature for 12 h under nitrogen atmosphere. PLGA-NHS was obtained by precipitation with cold diethyl ether (10 mL) as a white solid, which was filtered and repeatedly washed in a cold mixture of diethyl ether and methanol and then dried with nitrogen and under vacuum (yield, ~95%). The polymer activated PLGA-NHS (3.0 g, 0.166 mmol) was dissolved in anhydrous chloroform (10 mL), and NH_2-PEG-COOH (0.75 g, 0.22 mmol) and *N*,*N*-diisopropylethylamine (DIPEA) (42 mg, 0.75 mmol) were then added under magnetic stirring. The reaction mixture was magnetically stirred at room temperature for 24 h. The copolymer was obtained by treating the mixture with cold diethyl ether (yield, ~90%). The resulting PLGA-PEG block copolymer was dried under vacuum, characterized by ^{1}H NMR (500 MHz), and used for NP preparation without further treatment. ^{1}H NMR (500 MHz, $CDCl_3$): δ 5.23 (m, –OC– $CH(CH_3)$O–, PLGA), 4.78 (m, –OC–CH_2O–, PLGA), 3.65 (s, –CH_2CH_2O–, PEG), 1.56 (brs, –OCCHCH_3O–, PLGA).[49]

Nanoparticle Formulation

PCL:PLGA-PEG-COOH blend based NPs, with a mass ratio of 1.5:1, were prepared by a nanoprecipitation method. PCL, PLGA-PEG-COOH and RSV at three different concentrations (2, 3, and 4%, w/w, indicated as RSV1, RSV2, and RSV3, respectively) were dissolved in acetonitrile and added into water, under gentle stirring, giving a final polymer concentration of about 7.0 mg/ mL.

The resulting milky colloidal suspension was stirred at room temperature to remove the organic solvent. NPs were centrifuged at 10,000 rpm for 5 min and washed with water to remove the unencapsulated RSV. RSV-free NPs (RSV0) were produced in a similar manner and used as comparison.

The fluorescent FITC-loaded NPs were prepared using the above-mentioned procedure, by adding 0.67 mg of FITC instead of RSV. The obtained NPs suspension was used immediately for assay or lyophilized for storage at −50 °C.

Scanning Electron Microscopy (SEM) Analysis

Morphological examination of NPs was performed by scanning electron microscopy (SEM) (model DSM 962; Carl Zeiss Inc., Germany). A drop of NPs aqueous suspension was placed on an aluminum stub and dried under vacuum for 12 h. The samples were then analyzed at 20 kV acceleration voltage after gold sputtering, under an argon atmosphere.

Measurement of Particle Size and Polydispersity Index

Particle size (PS) and polydispersity index (PI) were measured at 25 °C using photon correlation spectroscopy (Zetasizer Nano ZS; Malvern Instruments, U.K.) at a temperature of 25 °C, and a scattering angle of 90° after dilution of formulations with Milli-Q water. Each sample was measured in triplicate.

Measurement of Zeta Potential

The zeta potential of NPs was measured at 25 °C with a Zetasizer Nano ZS under an electrical field of 40 V/cm. The samples were diluted with Milli-Q water and sonicated for several minutes before measurement. The data were obtained with the average of three measurements.

Drug Loading Content, Encapsulation Efficiency and Yield of Production

The amount of RSV encapsulated was determined by dissolving an aliquot of NPs (1.5 mg) in 1 mL of acetonitrile. The solution was filtered through a 0.2 μm syringe filter and analyzed by UV-vis spectroscopy (Cary 3, Varian) at 320 nm, and calculated by referring to the calibration curve (standard solutions in the range of 0.5–10 μg/mL; $R^2 = 0.9996$).

The drug loading content (DLC %), drug entrapment efficiency (EE %), and yield of NPs (YP %) were presented by the following equations, respectively:

DLC % = (weight of drug in NPs/weight of NPs) × 100

EE % (actual RSV content/theoretical RSV content) × 100

YP % (weight of NPs recovered/weight of polymer and RSV fed initially) × 100

Fourier Transform Infrared Spectroscopy (FT-IR)

The chemical composition of the RSV, PLGA-PEG-COOH, PCL, and RSV-loaded NPs was analyzed by FT-IR spectral measurements by using a Nicolet Nexus FT-IR spectrophotometer at a resolution of 4 cm^{-1} in KBr pellets, in the range 400–4000 cm^{-1}.

Thermal Analyses

The thermal properties of the empty and RSV-loaded NPs were determined using a differential scanning calorimeter (DSC) Q100 V 9.0 calorimeter (TA Instruments, New Castle, DE, USA). Indium was used to calibrate the instrument. The thermograms of samples were obtained at a scanning rate of 10 °C/min in 30–500 °C temperature range and performed under an Ar purge (50 mL/ min). The thermal measurements were carried out on pure RSV, PCL, and PLGA-PEG-COOH (raw materials), freeze-dried empty and RSV-loaded NPs, and the physical mixture of RSV, PCL, and PLGA-PEG-COOH. With the aim of determining the thermal stability of the samples, thermogravimetric analysis (TGA) was performed using a TGA Q5000IR (TA Instruments). Thermograms were obtained from 30 to 800 °C with a constant heating rate of 20 °C/min under air atmosphere, using aluminum crucibles with about 0.5 mg of each sample.

In Vitro Drug Release

Formulation RSV3, loaded with 4% w/w of RSV, was chosen, on the basis of EE% results, for the next step of the study.

The in vitro release test were carried out at different pH conditions:

- at pH 1.2 for 2 h followed by pH 7.4 for 5 h, to simulate gastric and intestinal fluids, respectively;
- in phosphate buffer solution (PBS) at pH 6.5 and 7.4 for 24 h, to mimic both the slightly acidic microenvironment of extracellular fluid in most tumors and the physiological conditions, respectively.

About 2.0 mg of RSV-loaded NPs and pure RSV were placed into dialysis bags and suspended in 20 mL of release medium under sink conditions, then incubated at 37 °C and stirred at 200 rpm. At predetermined time intervals, 1 mL of sample was withdrawn and replaced with an equal volume of the corresponding fresh medium to maintain a constant volume. Samples were filtered and RSV concentration was assayed spectrophotometrically at 320 nm, thus calculated by referring to the respective calibration curve with standard solutions in the range of 0.5–20 μg/mL: in 0.1 N HCl, pH 1.2 (R^2 = 0.9992); in PBS, pH 6.5 (R^2 = 0.9990) and pH 7.4 (R^2 = 0.9991). Each experiment was performed in triplicate.

Cell Culture

The prostate carcinoma DU-145, PC-3, and LNCaP cells were obtained from American Type Culture Collection (Manassas, VA, USA). The cells were cultured in RPMI 1640 and were maintained under standard cell culture conditions supplemented with 10% FBS and 1% penicillin/ streptomycin at 37 °C and 5% CO_2 environment.

Cell Growth and Viability Assay

The cell growth and viability were assessed by the 3-[4,5-dimethylthiazol-2-yl]-2,5-diphenyl tetrazoliumbromide (MTT) assay as described previously. Briefly, the cells were plated at 1 × 10^4 per well in 200 μL of complete culture medium. The next day, cells were treated with native drug or nano-RSVs for 72 h, at 10, 20, 30, and 40 μM equivalent RSV concentrations. Each concentration was repeated in 10 wells.

After incubation for the specified time at 37 °C in a humidified incubator, cell viability was determined. MTT (5 mg/mL in PBS) was added to each well and incubated for 2 h, after which the plate was centrifuged at 500g for 5 min at 4 °C. The MTT solution was aspirated from the wells using vacuum, and 0.2 mL of buffered DMSO was added to each well. After a 10 min mixing, the absorbance was recorded on a microplate reader at the wavelength of 540 nm. The effect of each agent on growth inhibition was assessed as percentage of cell viability in which vehicle-treated cells were taken as 100% viable. The experiment was repeated three times with similar outcomes.

Cellular Uptake

Fluorescence microscopy was utilized to examine the cellular uptake of the nano-RSVs. Cells were plated in a 2-chambered slide at 5,000 cells/well and allowed to grow for 18 h. Postattachment, the cells were incubated for 120 min with FITC-loaded NPs. Unbound micelles were removed by washing three times with PBS, the cells were mounted using Gold Antifade Reagent containing DAPI (Life Technologies, Grand Island, NY), and the mountant was allowed to cure overnight in the dark at room temperature. The images were examined under Nikon Eclipse Ti inverted microscope (Nikon Instruments, Inc., Melville, NY), and images were captured with a camera attached to the microscope. The experiment was repeated four times with similar results.

Statistical Analysis

All data were subjected to one-way analysis of variance (ANOVA) (GraphPadPrism, version 5.03). Individual differences were evaluated using a nonparametric post hoc test (Tukey's test) and considered statistically significant at $P < 0.05$.

RESULTS AND DISCUSSION

To obtain an efficient polymeric carrier suitable to be used for the encapsulation of bioactive RSV, we sought to prepare anosystems by a blend of two biocompatible polymers, PCL and PLGA-PEG-COOH conjugate. While PCL was commercially available, the diblock copolymer PLGA-PEG-COOH was synthesized by conjugating heterofunctional PEG, NH_2-PEG-COOH to PLGA-COOH, following a modified procedure.[49]

Synthesis and Characterization of Diblock Copolymer PLGA-PEG-COOH

PEGylation of PLGA NPs is a useful strategy to prevent rapid RES uptake and prolong the systemic circulation time by preventing opsonin binding to the NP surface.[42] Moreover, PEGylation strategy is conveniently used to increase the aqueous solubility and stability of PLGA, also reducing intermolecular aggregation and decreasing immunogenicity, as mentioned above. The preparation of PEGylated NPs has been previously investigated by several synthetic strategies, for example by coupling PEG to PLGA to obtain the starting polymer PLGA-PEG.[52] Thus, the diblock copolymer PLGA-PEG-COOH (Figure 1) was synthesized by conjugating heterofunctional PEG, NH_2-PEG-COOH to activated PLGA-COOH using standard carbodiimide/NHS-mediated chemistry, following a modified procedure previously reported.[49]

PLGA-COOH was reacted with EDC and NHS in CH_2Cl_2 at room temperature to activate the carboxylic acids to the ester PLGA-NHS. The structure of copolymer was confirmed by ^1H NMR spectroscopy (Figure 2).

From the analysis of the spectra, a signal pattern consisting of a peak centered at 3.65 ppm, corresponding to the PEG methylene protons, together with typical peaks at 5.23, 4.78, 1.56 ppm, of the PLGA, was detected. Furthermore, we confirmed an increased efficacy of PEG conjugation to PLGA, as previously described.[49,52,53]

Formulation of NPs

RSV is of great interest in nutrition and medicine due to its potential health benefits, and some recent research programs are devoted to investigating innovative formulation strategies in order to provide a controlled release and/or to improve its stability and bioavailability.[54,55]

In this study, we developed RSV loaded polymeric NPs as suitable carriers to be used in PCa therapy. The target nanosystems were successfully prepared by a simple nano-precipitation method using a blend of PLGA-PEG-COOH conjugate and PCL, loading different amounts of RSV, and were fully characterized and investigated for their morphology, particle size and zeta potential, encapsulation efficiency, FT-IR, thermal analyses, and in vitro release kinetic. The PLGA, selected owing to their biocompatibility and biodegradability, is extensively used for a variety of drug delivery systems as well as for targeted and nontargeted nanoparticulate systems.[41,53] Moreover, surface modifying NPs with PEG are widely known to reduce nonspecific interactions, to prolong circulation time, and to promote their accumulation in tumors due to the EPR effect.[44,52]

Among biodegradable polymers, PCL is suitable for controlled drug delivery due to its high permeability to many drugs and nontoxicity.[56] Furthermore, PCL shows an exceptional ability to form blends with other polymers that can allow tailoring mechanical properties and degradation kinetics.[57] Concerning the interaction between these polymeric components, during the formation of NPs, the PLGA block would interact with the PCL to form a hydrophobic core, while the hydrophilic PEG-COOH chains protrude from the particle surface to stabilize the core.

Morphological Examination

Figure 3 shows SEM images of unloaded NPs (a) and NPs loaded with 4% w/w of RSV (b), chosen as examples. Similar morphological aspects of NPs with distinct spherical shape and without a tendency to aggregate were observed.

Particle Size and Zeta Potential

The hydrodynamic diameter and zeta potential of NP batches are summarized in Table 1. The results indicated that the particle mean diameter is about 150 nm, independently of the initial RSV amount loaded. Besides, the nanoparticle dispersions exhibit a unimodal distribution, and polydispersity index (PI) values ranging from 0.110 to 0.146, typical of monodispersed systems.[58]

The zeta potential was negative for both loaded and unloaded NPs, as a result of the negatively charged carboxyl groups on the terminal of PLGA-PEG.

Drug Loading, Encapsulation Efficiency and Yield of Production

As reported in Table 2, the percentage of RSV content resulted as 1.55%, 2.21% and 3.95% for batches loaded with 2%, 3% and 4% of RSV, respectively. This finding suggests that the encapsulation of RSV into the polymeric matrix of NPs is dependent on the initial amount of RSV used.

The high incorporation capability of polymeric blended NPs, with EE values ranging from 74% to 99%, can be explained by taking into consideration the amphiphilic characteristics of the *RSV* molecule.[34] In fact, the presence of the hydrophobic PCL and PLGA moieties and the hydrophilic PEG-COOH chains promote a good accommodation of the drug molecules into the polymeric matrix. Moreover, the nanoprecipitation process ensures good yields of production ranging from 43% to 62%.

Fourier Transform Infrared Spectroscopy

The qualitative composition of NPs was investigated by FT-IR spectroscopy. As shown in Figure 4, for PCL, it is possible to detect strong bands such as the carbonyl stretching mode near 1725 cm^{-1}, and bands at 2949–2865, 1293, 1240, and 1190 cm^{-1} corresponding to CH_2, C–C, asymmetric COC, and OC-O stretching, respectively. The PLGA-PEG-COOH spectrum is coherent with the structure of the expected copolymer (Figure 4), which shows an absorption band at 3300–3500 cm^{-1}, assigned to the terminal hydroxyl groups, and bands around 3000 cm^{-1} and 2860 cm^{-1}, due to C–H stretch of CH_3 and CH_2, respectively. Moreover, the strong signal at 1757 cm^{-1} is assigned to C=O stretch, the absorption peaks at 1640 and 1556 cm-1 are associated to C=O and C-N of amide bond, and the band at 1190 cm^{-1} is due to C–O stretch. The spectrum of RSV is characterized by the olefinic bands at 1010-968 cm^{-1}, C–O stretching vibrations at around 1150 cm-1, the intense C–C olefinic stretching at 1585 cm^{-1}, and C–C aromatic double-bond stretching at 1610 cm^{-1} . To further support the proposed composition of RSV-NPs, overlapping signals corresponding to the above-mentioned materials (i.e., PCL, PLGA-PEG-COOH, and RSV) were thus detected for the corresponding sample.

Thermal Analyses

DSC experiments were performed to investigate the physical state of the RSV in the NPs, RSV and polymer interactions, and interpolymer interactions and mixture behavior. Figure 5a shows the DSC thermograms of pure RSV, PCL, and PLGA-PEG-COOH. The DSC curve of RSV exhibited the characteristic endothermic peak correspond-ing to the melting point at 269.80 °C[33] The DSC thermogram of semicrystalline PCL showed a melting endotherm (63.44 °C) with an enthalpy of 100.6 J/g, and an endothermic decomposition peak centered at 416.44 °C. In a DSC scan of amorphous PLGA-PEG-COOH copolymer an endothermic decomposition peak appeared at about 340.17 °C. In Figure 5b, the DSC scans of unloaded and loaded NPs clearly show that the melting endotherms of PCL decreases by about 5 degrees compared to the pure PCL, and enthalpy of fusion decreases to about 80 J/g. A considerable shifting of endothermic decomposition peak of PLGA-PEG-COOH is observed from 340 °C to about 310 °C.

The observed changes of thermal behavior are classically associated with miscibility of PCL with other polymers and indicate specific interactions between the two polymers physically blended in the NPs.[59] Similarly, the DSC scans of the physical mixture of polymers and RSV confirmed the presence of a shifting of decomposition peaks with respect to pure polymers.

However, the absence of melting peak of RSV in the loaded NPs suggests that entrapped RSV was dispersed molecularly as amorphous state into the polymer matrix.[37]

As shown in Figure 6, the weight loss at 180 °C is 2.2% and 0.5% for free NPs (a) and RSV-loaded NPs (b), respectively, demonstrating that the samples did not suffer appreciable thermal decomposition below this temperature. This suggests that both loaded and free NPs can be processed with thermal treatments below 180 °C under air atmosphere.

At higher temperature, three peaks are present in the weight loss derivative curves of both free and loaded NPs. These peaks correspond to three processes involved in the thermal decomposition of each sample. Interestingly, the temperatures associated with the decomposition of the loaded NPs (270, 360, and 470 °C) are higher than those corresponding to the decomposition of the free NPs (230, 350, and 460 °C). This finding may suggest that the thermal stability of NPs loaded with RSV is improved with respect to free NPs.

In Vitro Drug Release

In order to enhance RSV bioavailability, the development of controlled delivery systems is emerging as a promising strategy. As for route of administration, research has leaned toward oral forms as they allow easy chronic administration, but parenteral forms, which escape intestinal metabolism, are also envisaged for acute treatment.[60]

To evaluate the potential of prepared NPs for parenteral and oral administration, we performed the in vitro release test in different media, at pH 6.5 and pH 7.4, to mimic both the acidic tumoral microenvironment and the physiological conditions, respectively, and at pH 1.2 for 2 h followed by pH 7.4 for 5 h, to reproduce the upper and lower gastrointestinal tract.

The cumulative amount of RSV released from NPs at pH 6.5 and pH 7.4, is reported in Figure 7a and compared with the dissolution behavior of free RSV. Results showed that free RSV dissolved quickly, its concentration being, under the conditions used, much lower than the limit of its solubility in water.[60]

Nanoparticle formulations showed an overlapping of release profiles, suggesting that the pH of the medium did not significantly affect the release of RSV from nanosystems. In particular, NPs are characterized by a controlled release with only 55% of RSV released within 7 h. Moreover, at both pH values, a complete release of RSV is obtained after 24 h of the test.

The results of in vitro release test performed in gastrointestinal simulated fluids are depicted in Figure 7b. As previously noted, the free RSV dissolves completely within the first 60 min. NPs release about 55% of encapsulated RSV within the first 2 h in acidic medium, and their total RSV content within the subsequent 5 h at pH 7.4. Despite previous results, in these conditions the release rate of RSV from NPs is strongly influenced by the pH of the medium and results 2.2-fold higher at pH 1.2 than that at pH 7.4. To investigate the kinetics and mechanism of RSV release from NPs, the release data were fitted to zero order (Q =

k_0t), first order ($\ln(100 - Q) = \ln Q_0 - k_1t$), Higuchi ($Q = k_H t^{1/2}$), and Korsmeyer– Peppas models.[61]

Table 3 shows the correlation values (R^2) used as an indicator of the best fitting of the models considered for RSV-NPs in different media. For all tested conditions, the best linearity was found in Higuchi's equation plot. Besides, to understand the drug release mechanism, the first 60% drug release data was fitted to the Korsmeyer–Peppas exponential model $M_t/M_\infty = Kt^n$, where M_t/M_∞ is fraction of drug released after time t, K is kinetic constant, and n is release exponent, which characterizes the different drug release mechanism. The magnitude of the release exponent (n) indicates the release mechanism. The limits considered were $n \leq 0.43$ for a classical Fickian diffusion-controlled drug release, $n = 0.85$ for case II relaxation release transport, non-Fickian, zero order release, and values between $0.43 < n < 0.85$ can be regarded as an indicator of anomalous transport.[62]

The values of the release exponent in RSV release obtained ranged from 0.8177 to 0.8395, indicating a combination of both diffusion of the RSV in the hydrated matrix and dissolution of the polymer. It is well-known that aliphatic polyesters, such as PCL and PLGA, decompose through hydrolytic cleavage of the ester bond.[63]

When the NPs are exposed to medium (following the swelling of hydrophilic PEG chains surrounding the NP surface), it permeates the core of NPs, promoting the RSV diffusion through the polymeric matrix, and thus initiating hydrolytic cleavage of the polymeric blocks.

Furthermore, the increased release rate observed in simulated gastrointestinal fluid can be related to the faster degradation of PLGA in acidic conditions that further catalyzed the hydrolysis process.[64]

Cytotoxicity and Cellular Uptake of NPs

To evaluate the antiproliferative activity of RSV encapsulated into NPs, viability tests were performed on three different PCa cell lines, including the DU-145 (hormone-independent cells), PC-3 (hormone-independent line possessing dysfunctional androgen receptors), and LNCaP (hormone-sensitive cells), with moderate, high, and low metastatic potential, respectively.

Viability of DU-145 (a), PC3 (b), and LNCaP (c) cells cultured with RSV-loaded NPs (RSV3), after 72 h, in comparison with that of free RSV at the 10 μM, 20 μM, 30 μM and 40 μM equivalent dose, are presented in Figure 8.

On the whole, the results clearly demonstrated that RSV formulated in polymeric blended NPs were more effective against all cancer cell lines than free RSV, in a concentration-dependent manner. In general, differences in sensitivity toward both RSV and RVS-NP exposure were found for the tested tumor cells. With a calculated inhibition concentration to reduce cell viability of 50% (IC_{50}) of 16 μM and 18 μM, DU-145 and LNCaP cells (respectively) resulted about 2-2.2-fold more responsive than PC-3 (IC_{50} = 35.5 μM, for PC-3) when treated with RSV-NPs. A quite different trend was observed for the free RSV,

with higher IC_{50} values (IC_{50s} = 28.4, 47.4, and 50.7 μM, for DU-145, PC-3, and LNCaP, respectively) with respect to that of the nano-RSV. In particular, a dramatic enhancement in antiproliferative activity against LNCaP was found for nano-RSV with respect to the free counterpart. However, differences in cell sensitivity were found for both treatments at different dose concentrations. More specifically, the cell viability of DU-145, PC-3 and LNCaP was decreased of about 30%, 22%, and 12%, respectively, for nano-RSV at 10 μM concentration exposure, corresponding to a significant increase in antiproliferative activity (~15%, 16% and 31%), compared to an equivalent amount of free RSV. At 20 μM, RSV-NPs determined an enhanced growth inhibition of DU-145, PC-3 and LNCaP cells of ~69%, 40%, and 23%, respectively, thus resulting in a significant reduction of cell viability of about 40%, 13% and 31% with respect to that of free RSV. Interestingly, such a dose (i.e., 20 μM of RSV effective concentration) first evidenced the sensitivity between the tested cell lines after nano-RSV treatment, with the most consistent growth inhibition profile toward the androgen-independent DU-145 cells. Antiproliferative investigation conducted at 30 and 40 μM further confirmed the dose-dependent behavior, as mentioned above. In fact, at 30 μM concentration exposure, tested nano-RSV determined cell viability inhibition of ~78%, 45% and 30%, with enhanced activity of ~22%, 16% and 28% with respect to free RSV, toward DU-145, PC-3 and LNCaP, respectively. Finally, at 40 μM RSV concentration, treatment with both RSV-NPs and free RSV proved the highest cytotoxicity, showing a cell growth inhibition of ~82%, 52% and 40%, together with an improved efficacy of ~10%, 11% and 23% with respect to free RSV, against DU-145, PC-3 and LNCaP cells, respectively, exposed to equimolar amounts of free and loaded RSV.

On the other hand, no significant influence on cell viability was observed for the corresponding RSV-free NPs (RSV0), when evaluated considering the same concentration of the polymers as in RSV-NPs at 40 μM (data not shown).

The observed decrease of viability on PCa cell lines treated with NPs compared to free RSV may be explained considering that nanoparticulate systems up to about 100–200 nm can be internalized by receptor mediated endocytosis, and then release the RSV at intracellular locations, thus resulting in enhanced therapeutic action.[30,32]

To further support the correlation between antiproliferative activity of the RSV-loaded NPs with cellular uptake by the cancer cells, the internalization of FITC-loaded NPs, incubated for 2 h, was visualized by confocal laser scanning microscope (CLSM). In all PCa cell lines no significant differences of uptake and location of NPs were observed.

Figure 9 shows the confocal microscopic images of LNCaP cell uptake efficiency of RSV3, reported as example. It can be seen that NPs, after 2 h incubation, showed higher cellular uptake with strong fluorescence in both the cell cytoplasm and around the nucleus, confirming their internalization and sustained retention by the cancer cells.

CONCLUSION

In this work, the natural polyphenol RSV was effectively encapsulated into NPs based on PCL:PLGA-PEG-COOH blends as carriers for PCa prevention and therapy. Such

nanosystems provide a high RSV loading capacity and are able to control the release at different pH values, thus offering the possibility of the administration of nanosystems by parenteral and oral route. Nano-RSVs significantly improved the antiproliferative efficacy compared to that of free RSV in DU-145, PC-3, and LNCaP cell lines, that can be attributed to the maximized uptake between NPs and cells, resulting in enhanced accumulation through endocytosis. Interestingly, the androgen-independent DU-145 and hormone-sensitive LNCaP cell lines proved to be more responsive than PC-3 after nano-RSVs exposure.

Currently, strategies to conjugate NPs with small molecules targeting prostate membrane specific antigen (PSMA) aimed at maximizing efficacy of RSV toward PSMA positive cells, with strong implication on the PCa treatment, are being developed.

Acknowledgments

ACKNOWLEDGMENTS

The authors gratefully acknowledge the Regione Autonoma della Sardegna for financial support of Grant CRP 25920, “Development of novel targeted nanodevices for the prevention, diagnosis and treatment of prostate cancer”, awarded to M.S. within the frame of “Legge regionale n. 7/ 2007, promozione della ricerca scientifica e dell’innovazione tecnologica in Sardegna, - Annualita 2010”. The authors also thank Dr. Patrizio Salice for his help for TGA analyses, and the Company Purac Biomaterials (Gorinchem, Netherlands) for providing PLGA polymer. I.A.S. was supported by ACS Grant 120038-MRSG-11-019-01-CNE.

REFERENCES

1. Pervaiz S, Holme AL. Resveratrol: its biologic targets and functional activity. Antioxid. Redox Signaling. 2009; 11:2851–2897.
2. Delmas D, Jannin B, Latruffe N. Resveratrol: preventingproperties against vascular alterations and ageing. Mol. Nutr. Food Res. 2005; 49:377–395. [PubMed: 15830334]
3. Tennen RI, Michishita-Kioi E, Chua KF. Finding a Target for Resveratrol. Cell. 2012; 148:387–389. [PubMed: 22304906]
4. Campagna M, Rvas C. Antiviral activity of resveratrol. Biochem. Soc. Trans. 2010; 38:50–53. [PubMed: 20074034]
5. Das S, Das DK. Resveratrol: a therapeutic promise for cardiovascular diseases. Recent Pat. Cardiovasc. Drug Discovery. 2007; 2:133–138.
6. Rchard T, Pawlus AD, Iglesias ML, Pedrot E, Waffo-Teguo P, Merillon JM, Monti JP. Neuroprotective properties of resveratrol and derivatives. Ann. N.Y. Acad. Sci. 2011; 1215:103–108. [PubMed: 21261647]
7. Jang M, Cai L, Udeani GO, Slowing KV, Thomas CF, Beecher CW, Fong HH, Farnsworth NR, Kinghorn AD, Mehta RG. Cancer chemopreventive activity of resveratrol, a naturalproduct derived from grapes. Science. 1997; 275:218–220. [PubMed: 8985016]
8. Dorrie J, Gerauer H, Wachter Y, Zunino SJ. Resveratrol induces extensive apoptosis by depolarizing mitochondrial membranes and activating caspase-9 in acute lymphoblastic leukemia cells. Cancer Res. 2001; 61:4731–4739. [PubMed: 11406544]
9. Estrov Z, Shishodia S, Faderl S, Harris D, Van Q, Kantarjian HM, Talpaz M, Aggarwal BB. Resveratrol blocks interleukin-1beta-induced activation of the nuclear transcription factor NF-kappaB, inhibits proliferation, causes S-phase arrest, and induces apoptosis of acute myeloid leukemia cells. Blood. 2003; 102:987–995. [PubMed: 12689943]
10. Hsieh TC, Burfeind P, Laud K, Backer JM, Traganos F, Darzynkiewicz Z, Wu JM. Cell cycle effects and control of gene expression by resveratrol in human breast carcinoma cell lines with different metastatic potentials. Int. J. Oncol. 1999; 15:245–252. [PubMed: 10402233]
11. Mitchell SH, Zhu W, Young CY. Resveratrol inhibits the expression and function of the androgen receptor in LNCaP prostate cancer cells. Cancer Res. 1999; 59:5892–5895. [PubMed: 10606230]

12. Kuwajerwala N, Cifuentes E, Gautam S, Menon M, Barrack ER, Reddy GP. Resveratrol induces prostate cancer cell entry into s phase and inhibits DNA synthesis. Cancer Res. 2002; 62:2488–2492. [PubMed: 11980638]
13. Sengottuvelan M, Viswanathan P, Nalini N. Chemopreventive effect of trans-resveratrol—A phytoalexin against colonic aberrant crypt foci and cell proliferation in 1,2-dimethylhydrazine induced colon carcinogenesis. Carcinogenesis. 2006; 27:1038–1046. [PubMed: 16338953]
14. Oi N, Jeong CH, Nadas J, Cho YY, Pugliese A, Bode AM, Dong Z. Resveratrol, a red wine polyphenol, suppresses pancreatic cancer by inhibiting leukotriene Ahydrolase. Cancer Res. 2010; 70:9755–9764. [PubMed: 20952510]
15. Chen Z, Jin K, Gao L, Lou G, Jin Y, Yu Y, Lou Y. Antitumor effects of bakuchiol, an analogue of resveratrol, on human lung adenocarcinoma A549 cell line. Eur. J. Pharmacol. 2010; 643:170–179. [PubMed: 20599920]
16. Niles RM, McFarland M, Weimer MB, Redkar A, Fu YM, Meadows GG. Resveratrol is a potent inducer of apoptosis in human melanoma cells. Cancer Lett. 2003; 190:157–163. [PubMed: 12565170]
17. Opipari AW Jr. Tan L, Boitano AE, Sorenson DR, Aurora A, Liu J. R Resveratrol-induced autophagocytosis in ovarian cancer cells. Cancer Res. 2004; 64:696–703. [PubMed: 14744787]
18. Zoberi I, Bradbury CM, Curry HA, Bisht KS, Goswami PC, Roti JL, Gius D. Radiosensitizing and antiproliferative effects of resveratrol in two human cervical tumor cell lines. Cancer Lett. 2002; 175:165–173. [PubMed: 11741744]
19. She QB, Bode AM, Ma WY, Chen NY, Dong Z. Resveratrol-induced activation of p53 and apoptosis is mediated by extracellular-signal-regulated protein kinases and p38 kinase. Cancer Res. 2001; 61:1604–1610. [PubMed: 11245472]
20. Lee KW, Bode AM, Dong Z. Molecular targets ofphytochemicals for cancer prevention. Nat. Rev. Cancer. 2011; 11:211–218. [PubMed: 21326325]
21. Hsieh TC, Wu JM. Differential effects on growth, cell cyclearrest, and induction of apoptosis by resveratrol in human prostatecancer cell lines. Exp. Cell Res. 1999; 249:109–115. [PubMed: 10328958]
22. Shih A, Zhang S, Cao HJ, Boswell S, Wu YH, Tang HY, Lennartz MR, Davis FB, Davis PJ, Lin HY. Inhibitory effect of epidermal growth factor on resveratrol-induced apoptosis in prostate cancer cells is mediated by protein kinase C-alpha. Mol. Cancer Ther. 2004; 3:1355–1364. [PubMed: 15542774]
23. Ratan HL, Steward WP, Gescher AJ, Mellon JK. Resveratrol-a prostate cancer chemopreventive agent? Urol. Oncol. 2002; 7:223–227. [PubMed: 12504842]
24. Seeni A, Takahashi S, Takeshita K, Tang M, Sugiura S, Sato SY, Shirai T. Suppression of prostate cancer growth by resveratrol in the transgenic rat for adenocarcinoma of prostate (TRAP) model. Asian Pac. J. Cancer Prev. 2008; 9:7–14. [PubMed: 18439064]
25. Wang TT, Hudson TS, Wang TC, Remsberg CM, Davies NM, Takahashi Y, Kim YS, Seifried H, Vinyard BT, Perkins SN, Hursting SD. Differential effects of resveratrol on androgen-responsive LNCaP human prostate cancer cells in vitro and in vivo. Carcinogenesis. 2008; 29:2001–2010. [PubMed: 18586690]
26. Juan ME, Buenafuente J, Casals I, Planas JM. Plasmatic levels of trans-resveratrol in rats. Food Res. Int. 2002; 35:195–199.
27. Signorelli P, Ghidoni R. Resveratrol as an anticancer nutrient: molecular basis, open questions and promises. J. Nutr. Biochem. 2005; 16:449–466. [PubMed: 16043028]
28. Zhang L, Gu FX, Chan JM, Wang AZ, Langer RS, Farokhzad OC. Nanoparticles in medicine: therapeutic applications and developments. Clin. Pharmacol. Ther. 2008; 83:761–769. [PubMed: 17957183]
29. Khushnud T, Mousa SA. Potential Role of Naturally Derived Polyphenols and Their Nanotechnology Delivery in Cancer. Mol. Biotechnol. 2013; 55(1):78–86. [PubMed: 23371307]
30. Byrne JD, Betancourt T, Brannon-Peppas L. Active targeting schemes for nanoparticle systems in cancer therapeutics. Adv. Drug Delivery Rev. 2008; 60:1615–1626.
31. Sanna V, Siddiqui IA, Sechi M, Mukhtar H. Nano-formulation of natural products for prevention and therapy of prostate cancer. Cancer Lett. 2013; 334:142–151.

32. Jabir NR, Tabrez S, Ashraf GM, Shakil S, Damanhouri GA, Kamal MA. Nanotechnology-based approaches in anticancer research. Int. J. Nanomed. 2012; 7:4391–4408.
33. Sanna V, Roggio AM, Piccinini M, Silani S, Marceddu S, Mariani A, Sechi M. Development of novel cationic chitosan- and anionic alginate-coated poly(d,l-lactide-co-glycolide) nanoparticles for controlled release and light protection of resveratrol. Int. J. Nanomed. 2012; 7:5501–5516.
34. Sahoo SK, Panyam J, Prabha S, Labhasetwar V. Residual polyvinyl alcohol associated with poly(d,l-lactide-co-glycolide) nano-particles affects their physical properties and cellular uptake. J. Controlled Release. 2002; 82:105–114.
35. Siddiqui IA, Mukhtar H. Nanochemoprevention by bioactive food components: a perspective. Pharm. Res. 2010; 27:1054–1060. [PubMed: 20221894]
36. Siddiqui IA, Adhami VM, Chamcheu JC, Mukhtar H. Impact of nanotechnology in cancer: emphasis on nanochemopre-vention. Int. J. Nanomed. 2012; 7:591–605.
37. Sanna V, Sechi M. Nanoparticle therapeutics for prostate cancer treatment. Maturitas. 2012; 73:27–32. [PubMed: 22341739]
38. Sanna V, Roggio AM, Posadino AM, Cossu A, Marceddu S, Mariani A, Alzari V, Uzzau S, Pintus G, Sechi M. Novel docetaxel-loaded nanoparticles based on poly(lactide-co-caprolactone) and poly(lactide-co-glycolide-co-caprolactone) for prostate cancer treatment: formulation, characterization and cytotox-icity studies. Nanoscale Res. Lett. 2011; 6:260. [PubMed: 21711774]
39. Danhier F, Ansorena E, Silva JM, Coco R, Le Breton A, Preat V. PLGA-based nanoparticles: an overview of biomedical applications. J. Controlled Release. 2012; 161:505–522.
40. Sah H, Thoma LA, Desu HR, Sah E, Wood GC. Concepts and practices used to develop functional PLGA-based nanoparticulate systems. Int. J. Nanomed. 2013; 8:747–765.
41. Panyam J, Sahoo SK, Prabha S, Bargar T, Labhasetwar V. Fluorescence and electron microscopy probes for cellular and tissue uptake of poly(D, L-lactide-coglycolide) nanoparticles. Int. J. Pharm. 2003; 262:1–11. [PubMed: 12927382]
42. Panyam J, Zhou WZ, Prabha S, Sahoo SK, Labhasetwar V. Rapid endolysosomal escape of poly (DL-lactide-co-glycolide) nanoparticles: implications for drug and gene delivery. FASEB J. 2002; 16:1217–1226. [PubMed: 12153989]
43. Gref R, Minamitake Y, Peracchia MT, Trubetskoy V, Torchilin V, Langer R. Biodegradable long-circulating polymeric nanospheres. Science. 1994; 263:1600–1603. [PubMed: 8128245]
44. Owens DE III, Peppas NA. Opsonization, biodistribution, and pharmacokinetics of polymeric nanoparticles. Int. J. Pharm. 2006; 307:93–102. [PubMed: 16303268]
45. Acharya S, Sahoo SK. PLGA nanoparticles containing various anticancer agents and tumour delivery by EPR effect. Adv. Drug Delivery Rev. 2011; 63:170–183.
46. Shao J, Li X, Lu X, Jiang C, Hu Y, Li Q, You Y, Fu Z. Enhanced growth inhibition effect of resveratrol incorporated into biodegradable nanoparticles against glioma cells is mediated by the induction of intracellular reactive oxygen species levels. Colloids Surf., B. 2009; 72:40–47.
47. Guo L, Peng Y, Yao J, Sui L, Gu A, Wang J. Anticancer activity and molecular mechanism of resveratrol-bovine serum albumin nanoparticles on subcutaneously implanted human primary ovarian carcinoma cells in nude mice. Cancer Biother. Radiopharm. 2010; 25:471–477. [PubMed: 20735207]
48. Siddiqui IA, Adhami VM, Bharali DJ, Hafeez BB, Asim M, Khwaja SI, Ahmad N, Cui H, Mousa SA, Mukhtar H. Introducing nanochemoprevention as a novel approach for cancer control: proof of principle with green tea polyphenol epigallocatechin-3-gallate. Cancer Res. 2009; 69:1712–1716. [PubMed: 19223530]
49. Sanna V, Pintus G, Roggio AM, Punzoni S, Posadino AM, Arca A, Marceddu S, Bandiera P, Uzzau S, Sechi M. Targeted biocompatibile nanoparticles for the delivery of (-)-epigallocatechin 3-gallate to prostate cancer cells. J. Med. Chem. 2011; 54:1321–1332. [PubMed: 21306166]
50. Sanna V, Sechi M. Nanoparticle therapeutics for prostatecancer treatment. Nanomedicine. 2012; 8:S31–S36. [PubMed: 22640911]
51. Adhami VM, Malik A, Zaman N, Sarfaraz S, Siddiqui IA, Syed DN, Afaq F, Pasha FS, Saleem M, Mukhtar H. Combinedinhibitory effects of green tea polyphenols and selective cyclo-oxygenase-2 inhibitors on the growth of human prostate cancer cellsboth in vitro and in vivo. Clin. Cancer Res. 2007; 5:1611–1619. [PubMed: 17332308]

52. Betancourt T, Byrne JD, Sunaryo N, Crowder SW, Kadapakkam M, Patel S, Casciato S, Brannon-Peppas L. PEGylation strategies for active targeting of PLA/PLGA nanoparticles. J. Biomed. Mater. Res., Part A. 2009; 91:263–276.

53. Cheng J, Teply BA, Sherifi I, Sung J, Luther G, Gu FX, Levy-Nissenbaum E, Radovic-Moreno AF, Langer R, Farokhzad OC. Formulation of functionalized PLGA-PEG nanoparticles for invivo targeted drug delivery. Biomaterials. 2007; 28:869–876. [PubMed: 17055572]

54. Oganesyan EA, Miroshnichenko II, Vikhrieva NS, Lyashenko AA, Leshkov SY. Use of nanoparticles to increase thesystemic bioavailability of trans-resveratrol. Pharm. Chem. J. 2010; 44:25–27.

55. Peng H, Xiong H, Li J, Li J, Xie M, Liu Y, Bai C, Chen L. Vanillin cross-linked chitosan microspheres for controlled release of resveratrol. Food Chem. 2010; 121:23–28.

56. Sinha VR, Bansal K, Kaushik R, Kumria R, Trehan A. Poly-ε-caprolactone microspheres and nanospheres: an overview. Int. J. Pharm. 2004; 278:1–23. [PubMed: 15158945]

57. Dash TK, Konkimalla VB. Polymeric Modification and Its Implication in Drug Delivery: Poly-ε-caprolactone (PCL) as a Model Polymer. Mol. Pharmaceutics. 2012; 9:2365–2379.

58. Donini C, Robinson DN, Colombo P, Giordano F, Peppas NA. Preparation of poly(methacrylic acid-g-poly(ethyleneglycol)) nanospheres from methacrylic monomers for pharmaceuticalapplications. Int. J. Pharm. 2002; 245:83–91. [PubMed: 12270245]

59. Chun YS, Kyung YJ, Jung HC, Kim WN. Thermal andrheological properties of poly(ε-caprolactone) and polystyrene blends. Polymer. 2000; 41:8729–8733.

60. Amri A, Chaumeil JC, Sfar S, Charrueau C. Administration of resveratrol: What formulation solutions to bioavailability limitations? J. Controlled Release. 2012; 158:182–193.

61. Mehta AK, Yadav KS, Sawant KK. Nimodipine loaded PLGA nanoparticles: formulation optimization using factorial design, characterization and in vitro evaluation. Curr. Drug Delivery. 2007; 4:185–193.

62. Korsmeyer RW, Gurney R, Doelker E, Buri P, Peppas NA. Mechanism of solute release from porous hydrophilic polymer. J.Pharm. Sci. 1983; 15:25–35.

63. Cai Q, Shi G, Bei J, Wang S. Enzymatic degradationbehavior and mechanism of poly(lactide-co-glycolide) foams bytrypsin. Biomaterials. 2003; 24:629–638. [PubMed: 12437957]

64. de Jonga SJ, Ariasa ER, Rijkersb DTS, van Nostruma CF, Kettenes-van den Boschc JJ, Henninka WE. New insights intothe hydrolytic degradation of poly(lactic acid): participation of thealcohol terminus. Polymer. 2001; 42:2795–2802.

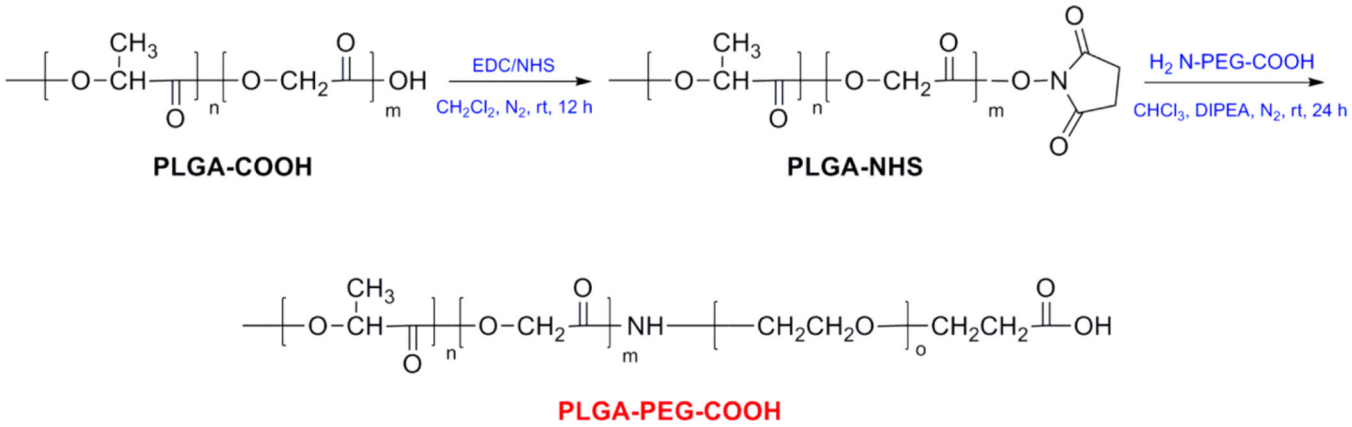

Figure 1.

Synthesis of copolymer PLGA-PEG-COOH. The starting carboxylate-functionalized diblock copolymer was synthesized by conjugating the heterofunctional PEG with a terminal amine and carboxylic acid functional group to PLGA-COOH, using standard carbodiimide/NHS-mediated chemistry.

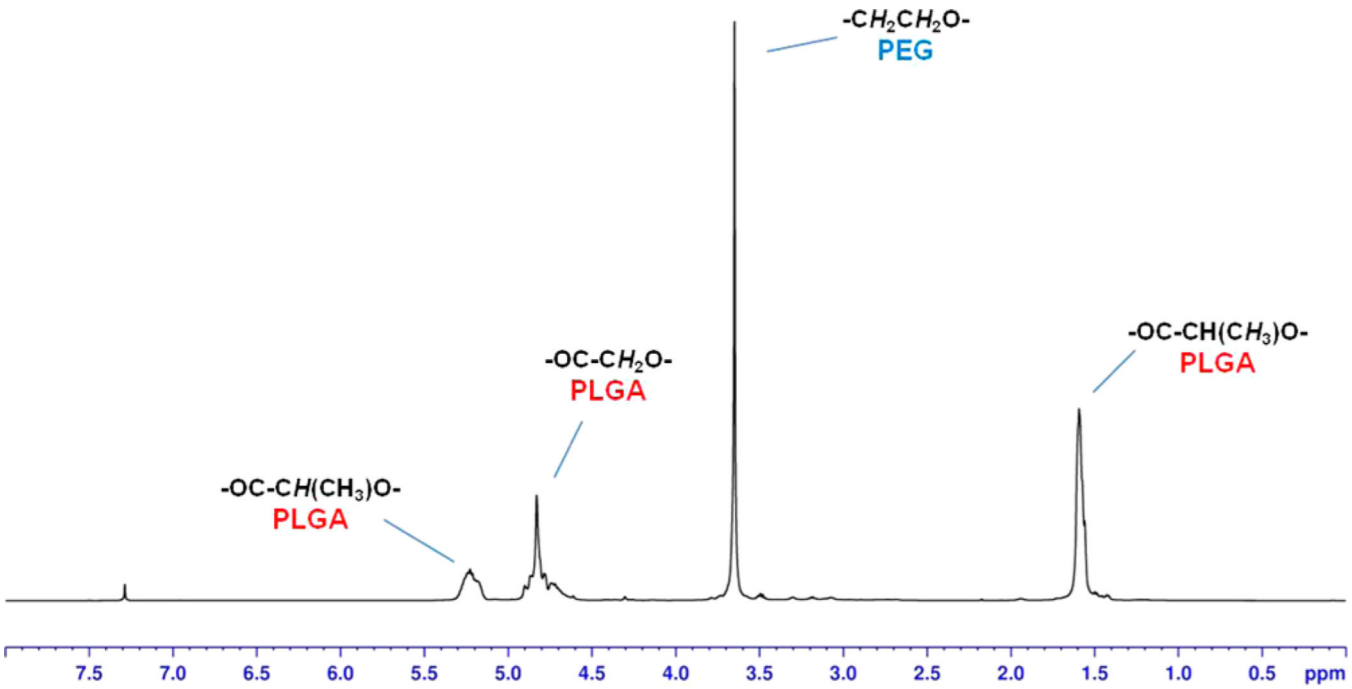

Figure 2.

^{1}H NMR with pattern signals of copolymer PLGA-PEG-COOH. A signal pattern consisting on a large peak centered at 3.65 ppm, corresponding to the PEG methylene protons, together with typical peaks at 5.23, 4.78, 1.56 ppm, of the PLGA, confirmed the structure of the copolymer.

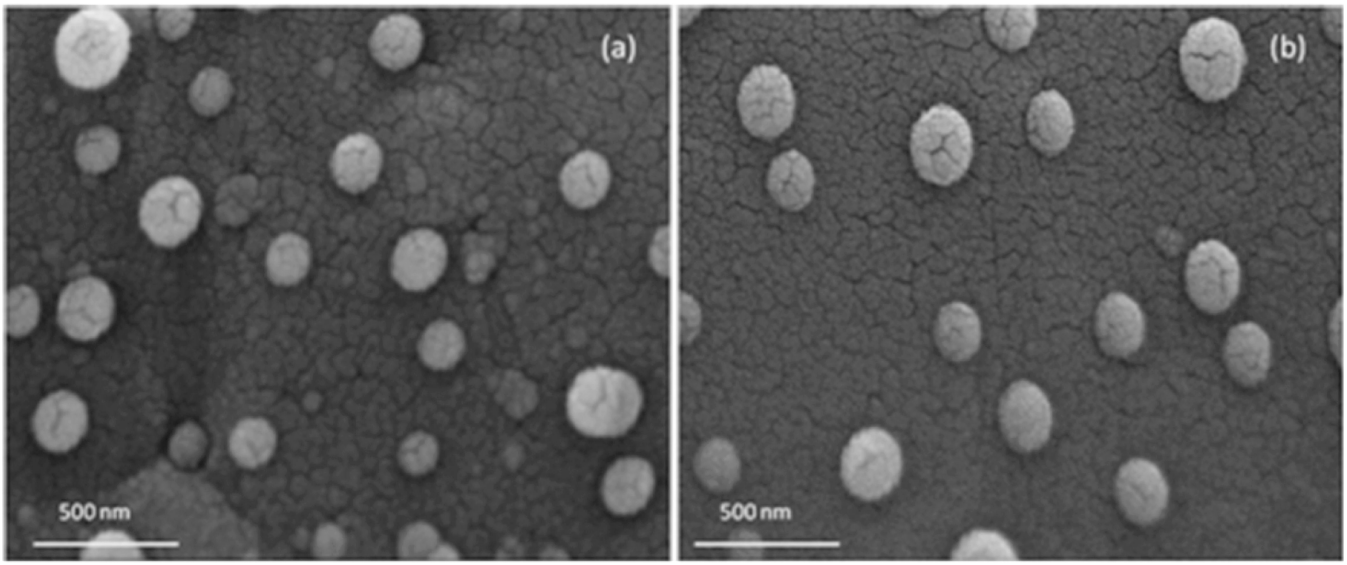

Figure 3.
SEM images of unloaded (a) and RSV-loaded (b) NPs. Particles were characterized by similar morphological aspects, with distinct spherical shape and without a tendency to aggregate.

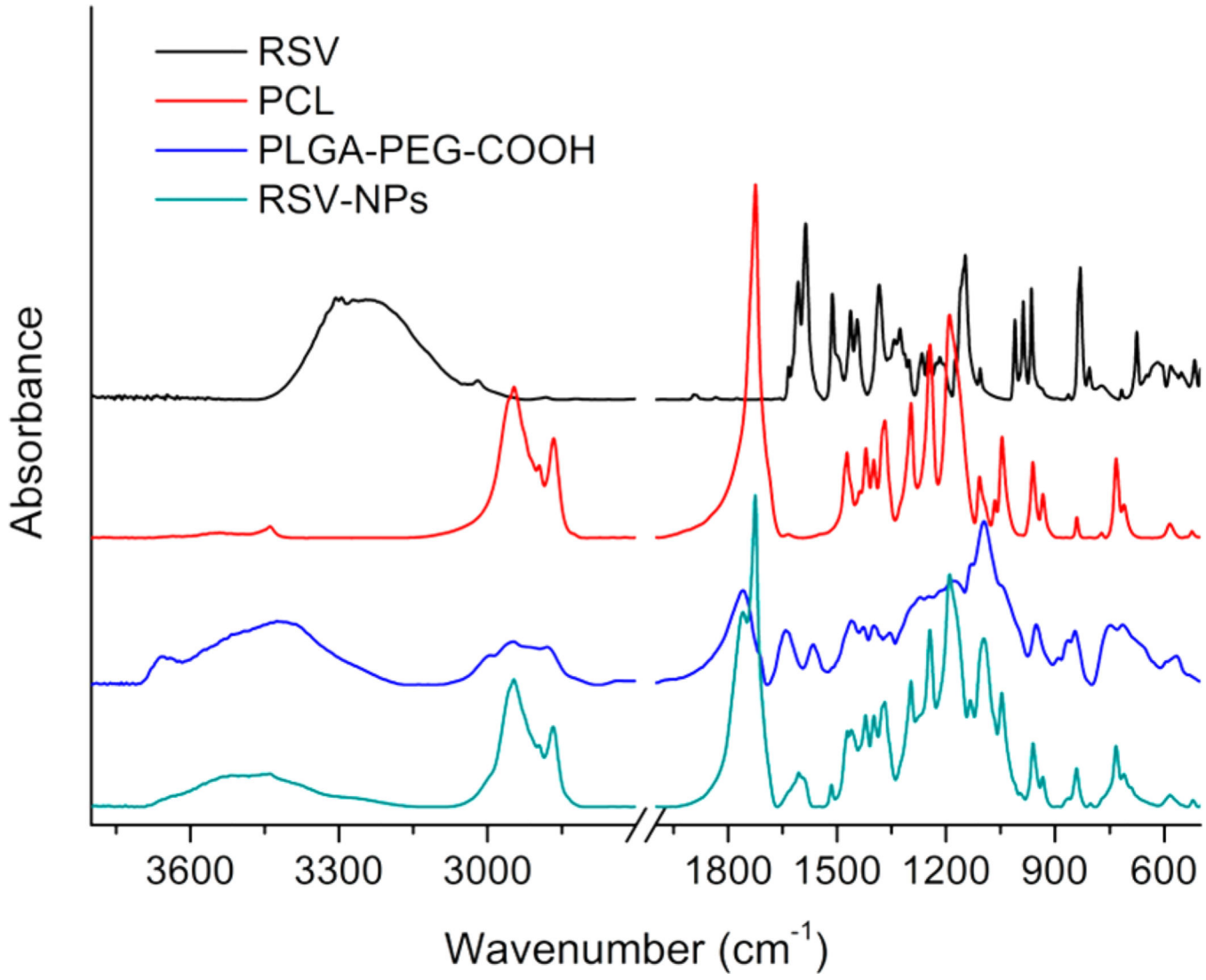

Figure 4.

FT-IR spectra of RSV, PLGA-PEG-COOH, PCL, and RSV-loaded NPs. To support the proposed composition of RSV-NPs, overlapping signals corresponding to the PCL, PLGA-PEG-COOH, and RSV were detected.

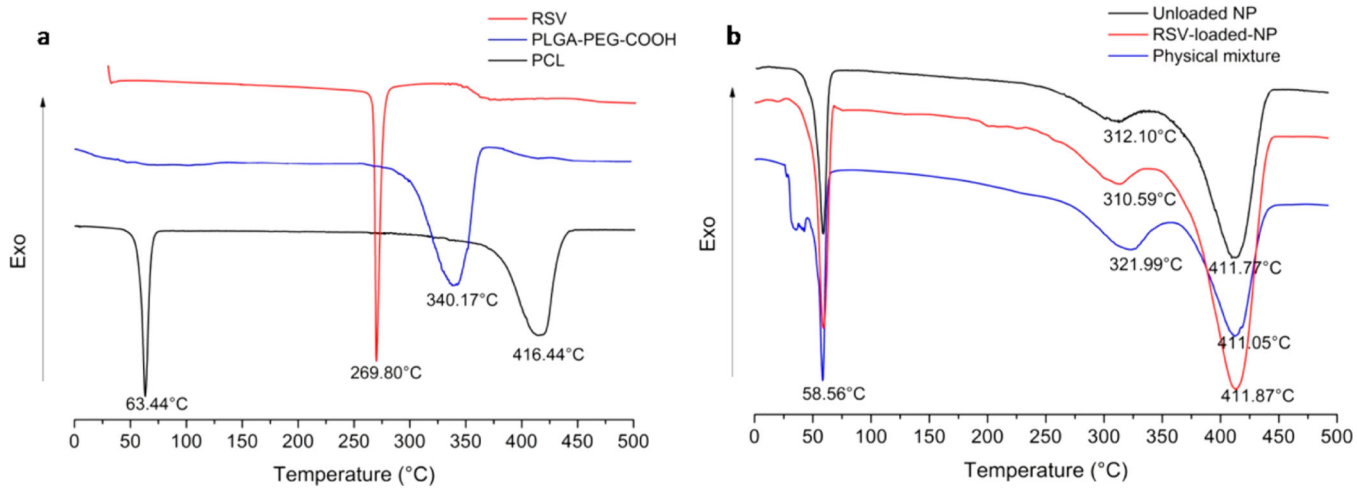

Figure 5.

DSC curves of (a) pure RSV, PLGA-PEG-COOH, PCL, and (b) unloaded NP, loaded NP, and physical mixture of RSV, PCL, and PLGA-PEG-COOH.

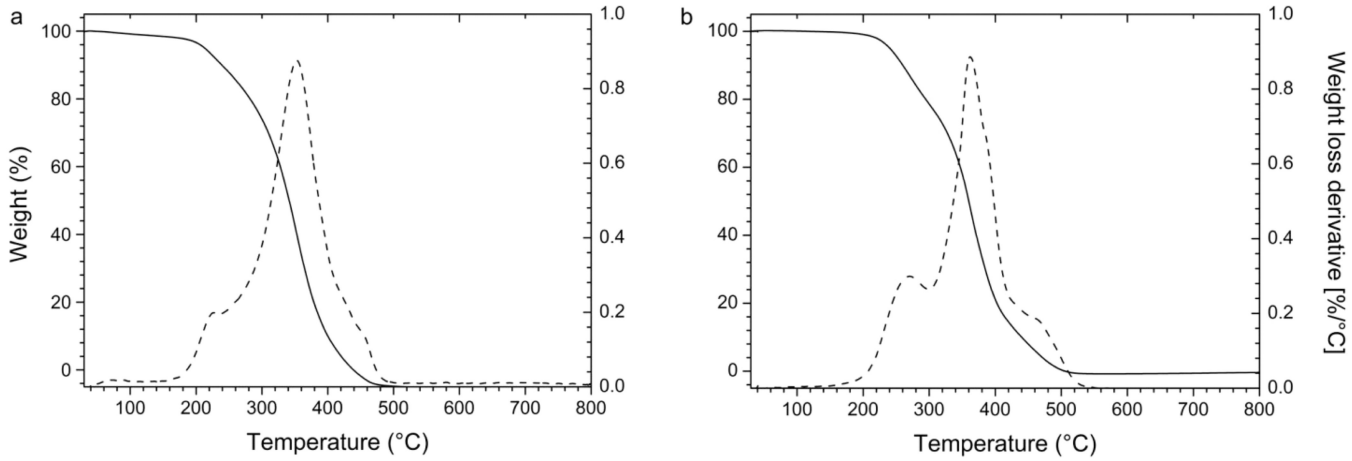

Figure 6.

Thermograms of free (a) and RSV-loaded (b) NPs (20 °C/min under air). Solid lines refer to weight (left axis) and dashed ones to weight derivative (right axis).

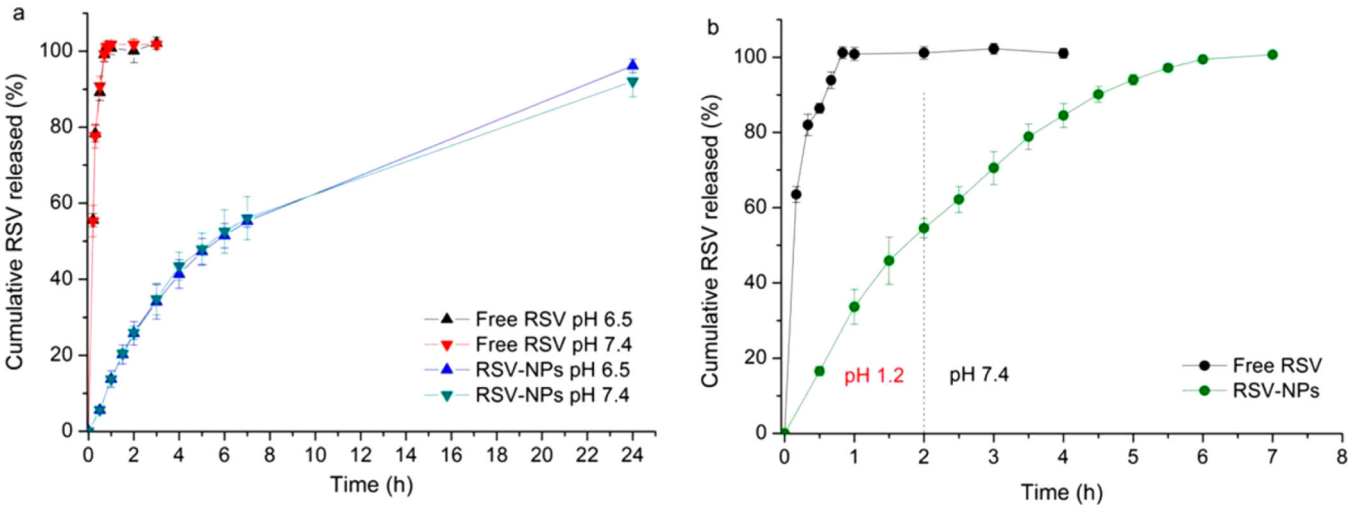

Figure 7.

In vitro release profiles of free RSV and RSV3 NPs: (a) in PBS, pH 6.5 and 7.4 performed for 24 h; (b) in 0.1 N HCl, pH 1.2 for 2 h followed by PBS, pH 7.4, for 5 h. Data are means ± SD, *n* = 3.

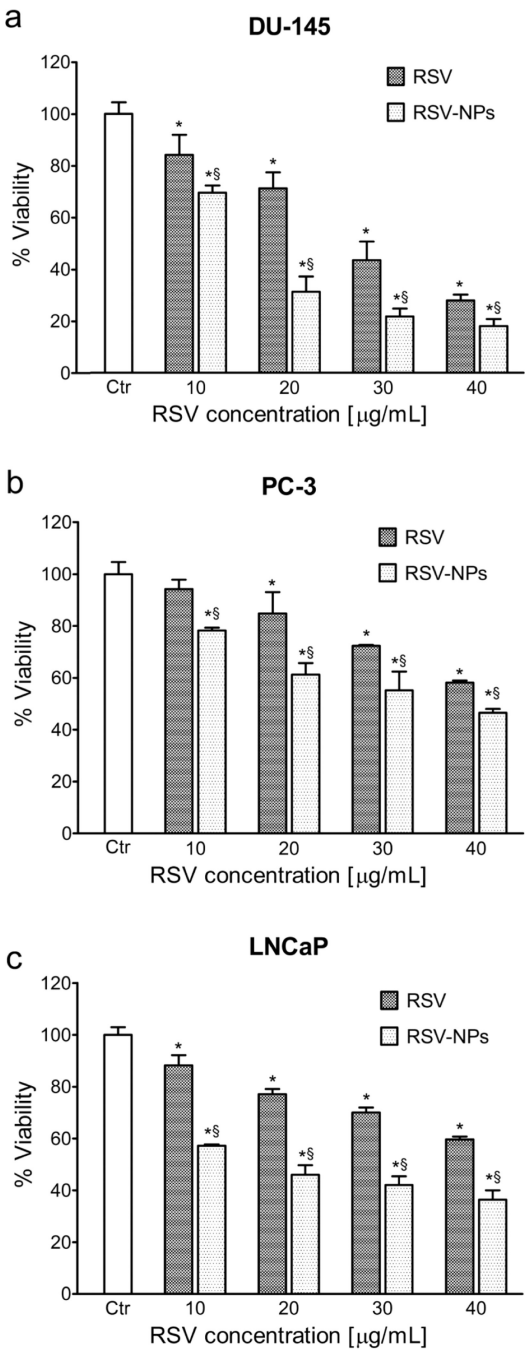

Figure 8.

Viability of DU-145 (a), PC3 (b), and LNCaP (c) cells cultured with RSV-loaded NPs (RSV-NP) after 72 h, in comparison with that of pure RSV at the 10 μM, 20 μM, 30 μM and 40 μM dose ($n = 3$). *Significantly different ($P < 0.05$) from control. §Significantly different ($P < 0.05$) from pure RSV at equivalent doses.

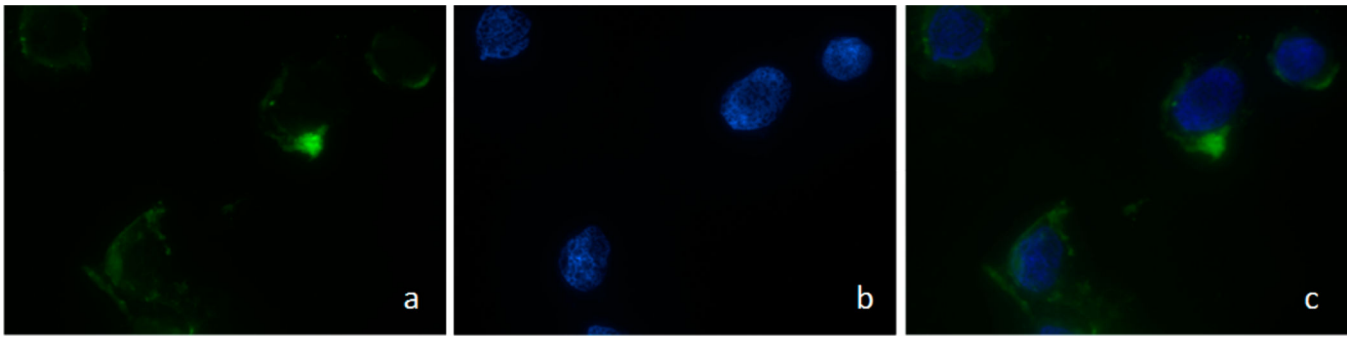

Figure 9.

Confocal laser scanning microscopy (CLSM) images of LNCaP cell lines, chosen as example, after 120 min incubation with FITC-loaded NPs at 37.0 °C. The cells were stained by DAPI (blue), and the FITC-loaded NPs are green. The cellular uptake was visualized by overlaying images obtained with both EGFP and DAPI filters: left image from EGFP channel (a); center image from DAPI channel (b); right image from combined EGFP and DAPI channels (c).

Table 1

Particle Size (PS), Polydispersity Index (PI), and Zeta Potential (ZP) of Formulated NPs[a]

batch	PS (nm) ± SD	PI ± SD	ZP (mV)
RSV0	150.80 ± 0.69	0.127 ± 0.01	−21.3 ± 8.35
RSV1	152.77 ± 0.70	0.119 ± 0.01	−24.2 ± 6.09
RSV2	150.70 ± 1.30	0.146 ± 0.01	−23.3 ± 7.20
RSV3	154.77 ± 0.21	0.110 ± 0.01	−29.7 ± 8.95

[a]Data are means ± SD, n = 3.

Table 2

Encapsulation Efficiencies (EE), RSV Loading Content (DLC), and Yields of Production (YP) of Formulated NPs[a]

batch	% EE ± SD	% DLC ± SD	% YP ± SD
RSV0			54.37 ± 3.24
RSV1	77.38 ± 2.25*	1.55 ± 0.04*	42.53 ± 3.72§
RSV2	73.80 ± 2.84#	2.21 ± 0.09*	52.40 ± 5.00*
RSV3	98.73 ± 0.98*#	3.95 ± 0.04*	62.00 ± 3.27*

a,*,# Significant differences ($P < 0.05$) between loaded NPs.

§ Significantly different from the unloaded NPs. Data are means ± SD, $n = 3$.

Table 3

Correlation Coefficients (R^2) and Release Exponent (n) of Kinetic Data Analysis of RSV Release from NPs in Different Media

	R^2			Korsmeyer-Peppas	
medium pH	**zero order**	**first order**	**Higuchi**	R^2	n
6.5	0.9568	0.9877	0.9948	0.9699	0.8323
7.4	0.9526	0.9849	0.9968	0.9708	0.8395
1.2/7.4	0.9611	0.9673	0.9961	0.9778	0.8177

Mol Pharm. Author manuscript; available in PMC 2014 July 16.